Experimental Study of the Premonitory Factors for Internal Erosion and Piping Failure of Landslide Dams

Austin Chukwueloka-Udechukwu Okeke, Fawu Wang, Yohei Kuwada, and Yasuhiro Mitani

Abstract

A good knowledge of sediment transport processes, including the hydraulics and hydrodynamics is prerequisite for a better understanding of the complex mechanisms of internal erosion and piping failure of landslide dams. To this end, a series of large-scale (outdoor) physical experiments were conducted to evaluate the premonitory factors and the critical conditions for piping failure of landslide dams. The experimental facility comprises a horseshoe-shaped trapezoidal barrier of length 8 m and height 2 m, with an open end for the construction of the dam models. Internal deformations associated with the onset of internal erosion were monitored with four strain gauges inserted into a PVC pipe and laid ~ 0.5 m above a 0.2 m-wide artificial drainage channel comprised of uniformly-sized pebbles and gravel. The rate of internal erosion and piping was measured with a turbidity sensor installed near the potential exit point of the seepage water to record the changes in turbidity of the fluidized sediments. Transient variations in the upstream reservoir were monitored with a 50 kPa capacity pore-pressure transducer while the hydrodynamic changes that occurred during the onset of internal erosion and piping were monitored with three pore-pressure transducers. The deformation behaviour of the dam models was monitored with two multi-function analog laser displacement sensors while self-potential measurements were made to track the development of the piping hole under steady-state flow conditions. The experimental results indicated that the emergence of an effluent seepage of high turbidity at the downstream face of the dam models coincided with high negative self-potential anomalies. This was also found to correlate with the development of high pore-water pressures (4–8 kPa) which subsequently led to a gradual decrease in the dam height (settlement). These large-scale (outdoor) physical experiments provide important information which may be useful in estimating the breaching process of landslide dams as triggered by piping.

Keywords

Physical experiments • Landslide dams • Turbidity • Monitoring sensors • Internal erosion • Piping

A.C.-U. Okeke (✉)
Department of Civil Engineering, College of Engineering, Covenant University, Ota, Ogun State, Nigeria
e-mail: chukwueloka.okeke@covenantuniversity.edu.ng

A.C.-U. Okeke · F. Wang · Y. Kuwada · Y. Mitani
Research Center on Natural Disaster Reduction, Shimane University, 1060 Nishikawatsu-Cho, Matsue, Shimane 690-8504, Japan
e-mail: wangfw@riko.shimane-u.ac.jp

Introduction

The occurrence of landslides and rock avalanche processes can result in the natural damming of stream channels and gorges. Such events are common in many mountainous regions where several geomorphological and hydro-climatic factors favour the occurrence of many geomorphic processes

that form landslide dams (Hewitt 1982; Hermanns et al. 2004). Once a landslide dam is formed, breaching could occur and result in the release of the impounded lake upstream of the dam. This oftentimes triggers catastrophic outburst floods that could potentially cause a lot of disasters in the downstream areas (Evans 1986; O'Connor and Beebee 2009). The probability of failure of landslide dams remains an integral part of flood risk modeling and natural hazard assessment studies. Costa and Schuster (1988) reported that the longevity of landslide dams depends on several factors including the rate of seepage through the dam; the internal structure and material properties of the dam; the size, shape, and volume of the blockage; and the rates of sediment and water flow into the upstream lake. Therefore, a better understanding of the premonitory factors for internal instability and failure of landslide dams is essential for flood risk assessment and natural disaster prevention.

Internal erosion and piping are among the major failure modes of landslide dams. Information on seepage processes (seepage velocity, seepage forces, seepage paths and hydraulic conductivity) are essential for predicting the hydraulic behaviour and the failure mechanisms of landslide dams. The vulnerability of landslide dams to seepage and internal erosion has been related to their internal structure and material properties (Strom 2006, 2013; Okeke and Wang 2016a). The formation of a lake upstream of a landslide dam can lead to the development of high seepage pressures that may initiate internal erosion which could progress to form a piping hole. Seepage triggers instability in landslide dams by: (1) causing a reduction in the resisting forces of the dam materials by increasing the pore-water pressure, (2) the evolution of seepage gradient forces that tend to pull the soil particles apart, and (3) mobilization and downstream entrainment of soil particles towards an unprotected exit. Landslide dams are predominantly unsaturated or partially saturated, and hence the presence of matric suction (negative pore-water pressure) induces an apparent cohesion that increases the stability of landslide dams. However, an increase in pore-water pressure results in the reduction of matric suction which in turn results in internal instability and failure (Okeke and Wang 2016b).

Predicting the premonitory conditions for the initiation of internal erosion and piping has been a major concern to geomorphologists and hydraulic engineers. Numerous attempts have been made to evaluate the complex mechanisms of internal erosion and piping in landslide dams and other hydraulic structures (Ojha et al. 2008; Amaya et al. 2009; Vorogushyn et al. 2009). Therefore, the main objectives of this research are to evaluate the premonitory factors for internal erosion and piping failure of landslide dams and to obtain a better understanding of their failure mechanisms as triggered by piping. These objectives were achieved by performing large-scale (outdoor) physical experiments using

different kinds of precision sensors and geophysical techniques to obtain real time data representative of the deformation behaviour of the dams.

Experimental Setup

The experimental facility comprises a horseshoe-shaped trapezoidal barrier of length 8 m and height 2 m, with an open end for the construction of the dam models (Fig. 1). The barrier was constructed such that the internal and external slope ratios were $1H : 1V$ and $1.5H : V$, respectively. The upstream lake was recharged from a drainage hose connected to a local water main. The deformation behaviour of the dam models was monitored with two multi-function analog laser displacement sensors suspended by a cylindrical metallic rod. The two sensors were separated by a horizontal distance that varied from 1 to 1.5 m in all the experimental runs. The rate of internal erosion and piping was measured with a turbidity sensor (model: VisoTurb[R] 700 IQ SW) installed near the potential exit face of the seepage water to record transient changes in turbidity of the fluidized sediments. Transient variation in the upstream reservoir was monitored with a 50 kPa capacity pore-pressure transducer, while the hydrodynamic changes that occurred during the onset of internal erosion and piping were monitored with three pore-pressure transducers. The three transducers hereinafter referred to as *PWP-1*, *PWP-2*, and *PWP-3* were inserted into a PVC pipe of diameter, 0.075 m, and laid above the artificial drainage channel. Internal deformations associated with the onset of internal erosion were monitored with four strain gauges inserted into a PVC pipe and laid at about 0.5 m above the artificial drainage channel. Two high-speed recording cameras were strategically positioned at different locations to capture the deformation behaviour of the dam models. The internal structure of the dam models before and after the experiments was evaluated by conducting microtremor chain array surveys along the dam crest. Self-potential measurements were also made along the dam crest to monitor the onset of internal erosion and piping. All these sensors were connected to a standard real-time monitoring and recording unit comprised of a universal recorder (KYOWA EDX-100A) and a laptop computer.

Test Preparation and Dam Model Construction

A series of large-scale (outdoor) landslide dam models were constructed using a mini-excavator and hand-propelled vibratory plate compactor. The materials used in building the dam models consist of highly weathered igneous and

Fig. 1 Setup of the experimental dam prior to the commencement of an experiment
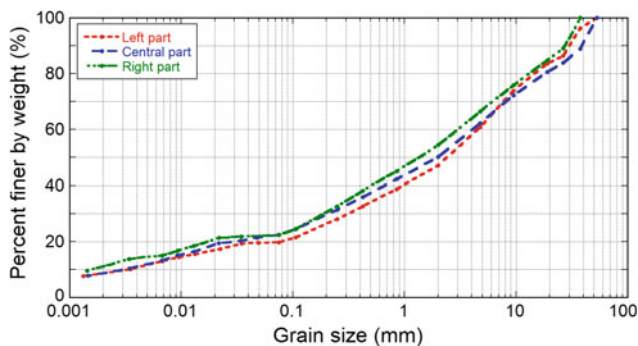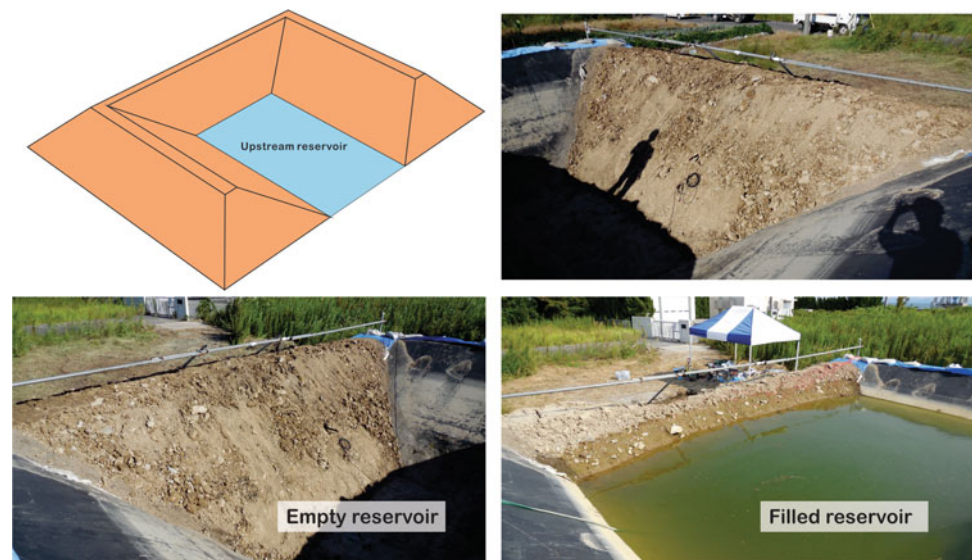

Fig. 2 Grain size distribution curves of the dam material sampled at three different locations

sedimentary rocks including ferruginized sandstone and mudstone. The grain size distribution curves of the material are shown in Fig. 2. The soil consists of 35.5% gravel, 37.5% sand, 20.9% silt and 6.1% clay-sized particles, with an average coefficient of curvature, coefficient of uniformity and effective grain size of 0.686, 93.33 and 0.015 mm, respectively. Internal erosion was initiated by laying uniform gravel and cobbles in a 0.2-m wide rectangular channel (Fig. 3a). Subsequently, the material used in building the dam models was placed in equal lifts and then compacted with a hand-propelled vibratory plate compactor. The geometrical characteristics of the dam models are shown in Fig. 3b. The dam height, H_d and the dam crest width, D_{crw} ranged from 1.7 to 2 m and 0.8 to 0.95 m, respectively, while α and β which represent the upstream and downstream slope angles were varied from 38 to 41° and 37 to 38°, respectively.

The experiments started with the filling of the upstream reservoir. The discharge into the reservoir was maintained until the reservoir level reached a maximum level considered safe for the operation of the dam. Subsequently, an equilibrium hydraulic head was maintained by establishing a static water level. In all the experimental runs, a large channel was excavated at the toe of the downstream slope to minimize backwater flooding and to ensure accurate readings from the turbidity sensor.

Results and Discussion

Experiment 1

Figure 4a shows the evolution of a piping hole and the deformation behaviour of the dam model used in *Experiment 1*. The dam material was partially saturated prior to the filling of the upstream reservoir, and hence the stability of the dam was controlled by the presence of negative pore-water pressure. The filling of the upstream reservoir induced the development of transient seepage through the dam due to a steady rise in the upstream lake. The early stages of initiation of internal erosion in the dam involved an abrupt drop in pressure of the seeping water through the upstream side of the artificial drainage channel.

The buildup of significantly high positive pore-water pressures and the subsequent reduction of the effective stress of the soil in the periphery of the drainage channel initiated minor internal deformations. Consequently, the reduction of the shear strength of the soil due to an increase in seepage gradient forces along the drainage channel resulted in soil particle mobilization and entrainment towards the downstream face. The internal erosion process progressed into piping as evidenced by the gradual outwash of hyperconcentrated flows from a poorly developed hole at the toe of the downstream face ("A" in Fig. 4a). This was followed by

Fig. 3 **a** Early stages of dam model construction and laying of artificial drainage channel **b** geometrical characteristics of the dam models
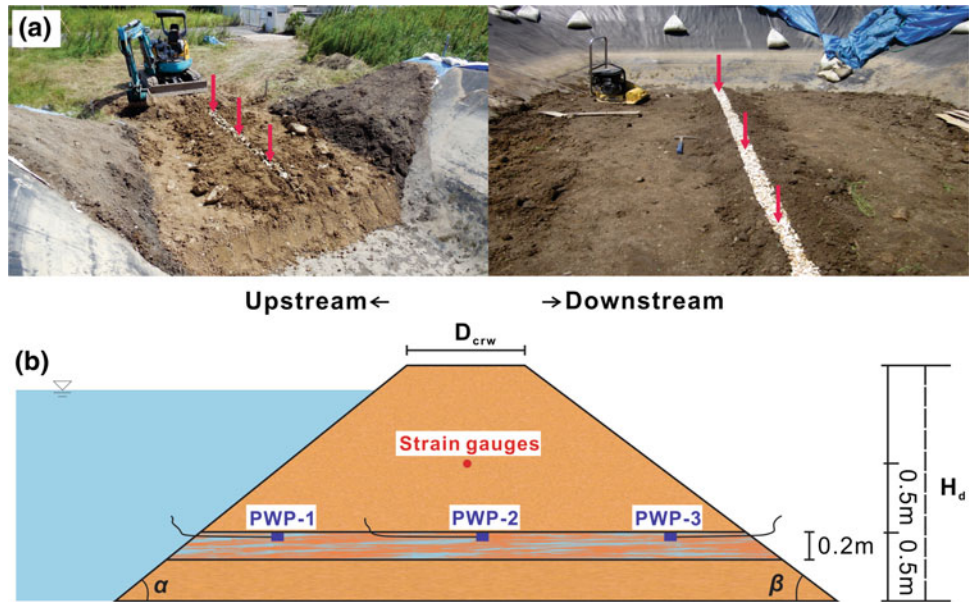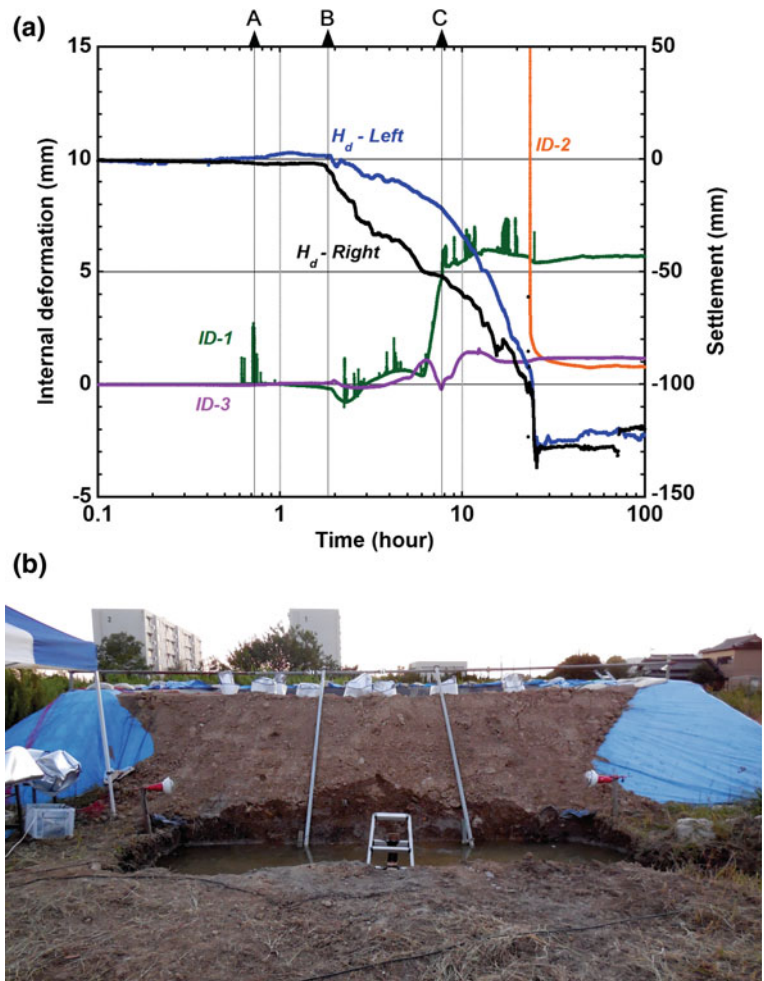

Fig. 4 **a** Deformation behaviour and evolution of a piping hole in *Experiment 1*. **b** Gradual undercutting of the downstream slope under steady-state seepage

a steady propagation of the wetting front and a gradual decrease in the dam height ("*B*" in Fig. 4a). The erosion processes that led to the evolution of the piping hole caused further (internal) deformations which resulted in the gradual undercutting of the downstream toe under steady-state saturation of the dam face ("*C*" in Fig. 4a, b). It is interesting to note that the outwash of the fluidized sediments from the evolving pipe coincided with the internal deformations recorded by the strain gauges. This indicates the effects of the erosive forces of the flowing water in the gradual reduction of the shear strength of the dam material.

Figure 5a shows the transient changes in turbidity of the hyperconcentrated flow and the deformation behaviour of the dam model. At the initial stage, the turbidity of the effluent seepage was lower than 55 NTU. However, the evolution of the piping hole at the downstream face caused the turbidity value to increase from 55 to about 70 NTU ("*A*" in Fig. 5a). This phenomenon marked the early onset of piping in the dam. This was followed by a rapid increase in turbidity of the hyperconcentrated flow, indicating the progression of internal erosion and piping through the dam ("*B*" in Fig. 5a). The rate of enlargement of the piping hole under intense erosion can be directly related to the gradual decrease in height of the dam due to the removal of the underlying material. The pipe enlargement process peaked with a sharp decrease in dam height which corresponded with high values of turbidity that ranged from 350 to 400 NTU ("*C*" in Fig. 5a). Pore-water pressure data obtained from the last stages of the test revealed that the values of *PWP-1* and *PWP-3* were as high as 11.8 and 8.7 kPa, respectively, while the corresponding critical hydraulic gradients for collapse of the dam crest (i_{f1} and i_{f2}) were 4.3 and 3.2, respectively (Fig. 5b).

Figure 6 summarizes the time-dependent deformation mechanism of the dam model. The emergence of the seepage water at the downstream face triggered further saturation and undercutting of the downstream toe that resulted in the evolution of several cracks on the dam crest (Fig. 6a–c). The inability of the piping hole to evolve into a larger hole can be attributed to the low plasticity nature of the dam material. Hence, failure was mostly triggered by dam face saturation, hydraulic cracking, settlement, downstream toe undercutting and progressive unraveling (Fig. 6d).

Experiment 2

Figure 7 shows the time-dependent deformation mechanism of the dam model under steady-state seepage conditions. The gradual rise in reservoir level and the subsequent increase in pore-water pressures caused internal stress redistribution that
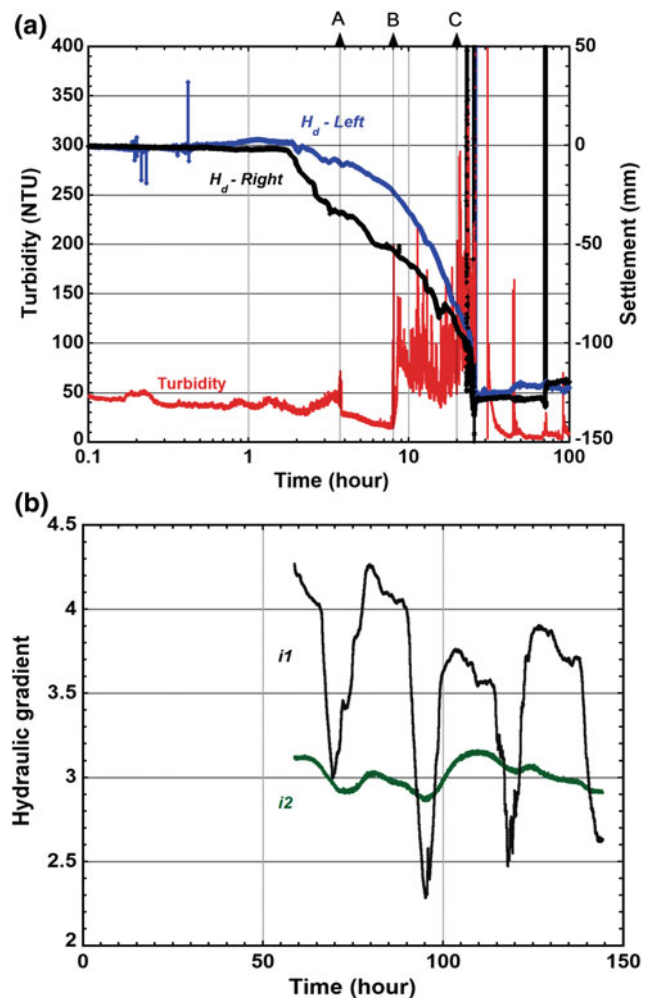

Fig. 5 a Deformation behaviour and transient changes in turbidity of the seepage water. **b** Trends of hydraulic gradients (i_{f1} and i_{f2}) during the experiment

resulted in the formation of concave upward depressions (settlements) on the dam crest ("*A*" in Fig. 7).

The low plasticity index of the dam material may have contributed to the high susceptibility of the dam to internal erosion. Early onset of internal erosion was detected by the strain gauges laid above the artificial drainage channel. The increase in seepage gradient forces within the artificial drainage channel triggered particle mobilization and entrainment that resulted in further redistribution of internal stresses as recorded by the strain gauges ("*B*" in Fig. 7). The onset of piping was marked by the emergence of very turbid seepage water from the downstream toe, which caused the turbidity of the seepage water to sharply increase from 40 to 270 NTU ("*A*" in Fig. 8).

The variation in turbidity of the effluent seepage is an indication of the episodic erosive action of the seepage
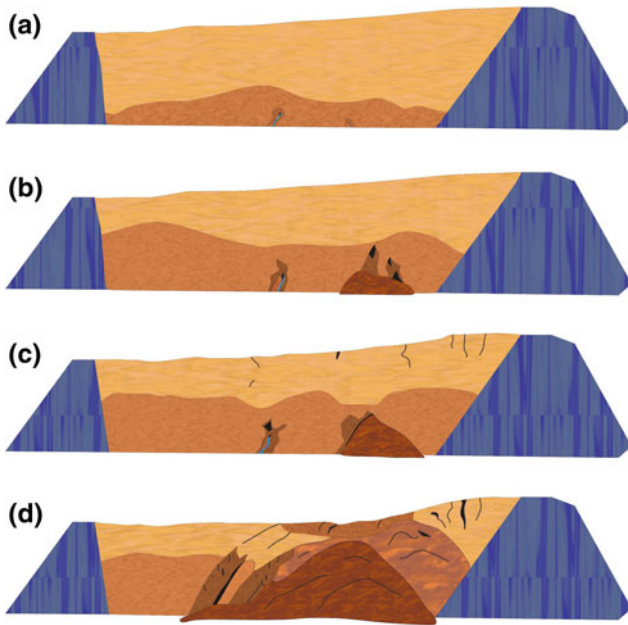
Fig. 6 Deformation mechanism of the dam model. **a** Seepage and upslope prepagation of the wetting front. **b** Evolution of a poorly developed piping hole. **c** Crest settlement and hydraulic cracking. **d** Downstream toe unraveling and sloughing
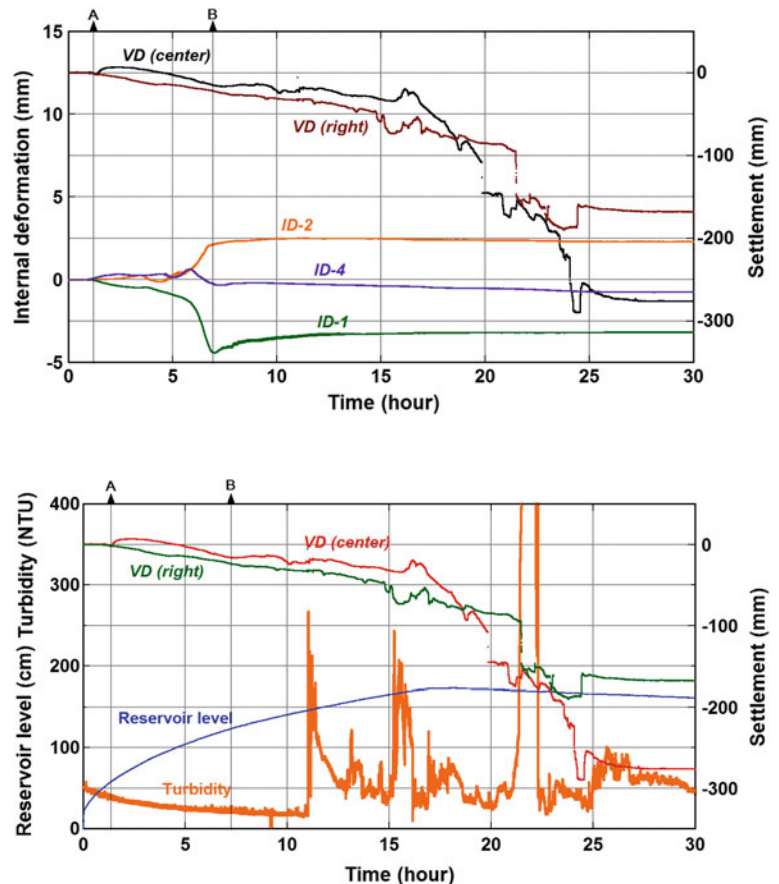
water. It is worthy to mention that the characteristic physical properties of the dam materials could not support the formation of a continuous piping hole through the dams. Hence, seepage was the primary failure mechanism. The inability of the dam materials to support the roof of the piping hole hindered further enlargement of the pipe. Consequently, the saturation of the downstream face under steady-state seepage resulted in the gradual undercutting of the downstream toe, leading to slope instability and progressive failure (lateral spread). This phenomenon is associated with very high turbidity values ("*B*" in Fig. 8) caused by the erosion and downstream transport of the mobilized materials.

Experiment 3

Figure 9 shows the trends of pore-water pressures and turbidity in the dam model used in *Experiment 3*. The dam was built to a height and dam crest with of 1.98 and 0.89 m, respectively, while the upstream and downstream slope angles were 41 and 38°, respectively.
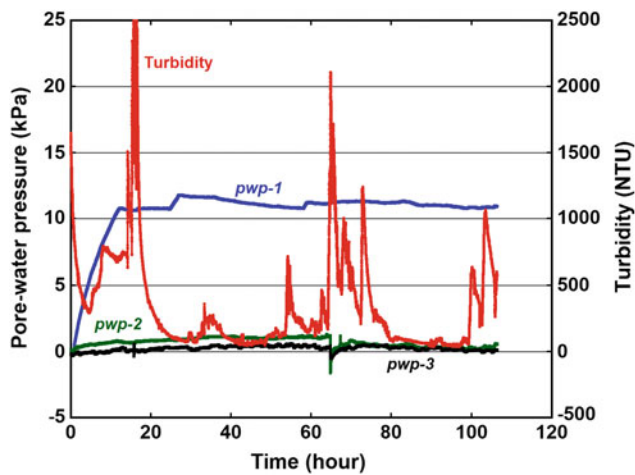
Fig. 7 Deformation behaviour of the dam model in *Experiment 2* under steady-state seepage conditions

Fig. 8 Stage hydrograph and transient variation in turbidity of the seepage water during *Experiment 2*

Fig. 9 Trends of pore-water pressures and variation in turbidity of the seepage water during *Experiment 3*

The rapid rise in pore-water pressures through the dam resulted in the development of high seepage gradient forces that caused abrupt erosion and outwash of the dam materials to an exit point on the downstream face. This is evidenced by the rapid increase in turbidity of the effluent seepage to about 2500 NTU. The evolution of seepage at the exit face of the downstream slope resulted in the upslope propagation of the wetting front, leading to progressive sloughing and settlement of the dam crest. The gradual undercutting and sloughing of the downstream slope under steady-state seepage further triggered several cycles of turbidity flows with peaks which varies from 1100 to 2200 NTU.

Figure 10a shows the trends of hydraulic gradients and the deformation mechanism of the dam model under steady-state seepage conditions. The measured critical hydraulic gradient for the collapse of the dam crest (i_{f2}) was found to coincide with the high turbidity of the seepage water, and thus indicates the early onset of internal instability of the dam (Fig. 10b). Further increase in i_{f2} was associated with a gradual deformation of the dam crest. Consequently, failure was generally triggered by downstream slope saturation, undercutting and sloughing of the fluidized materials as shown in Fig. 11.
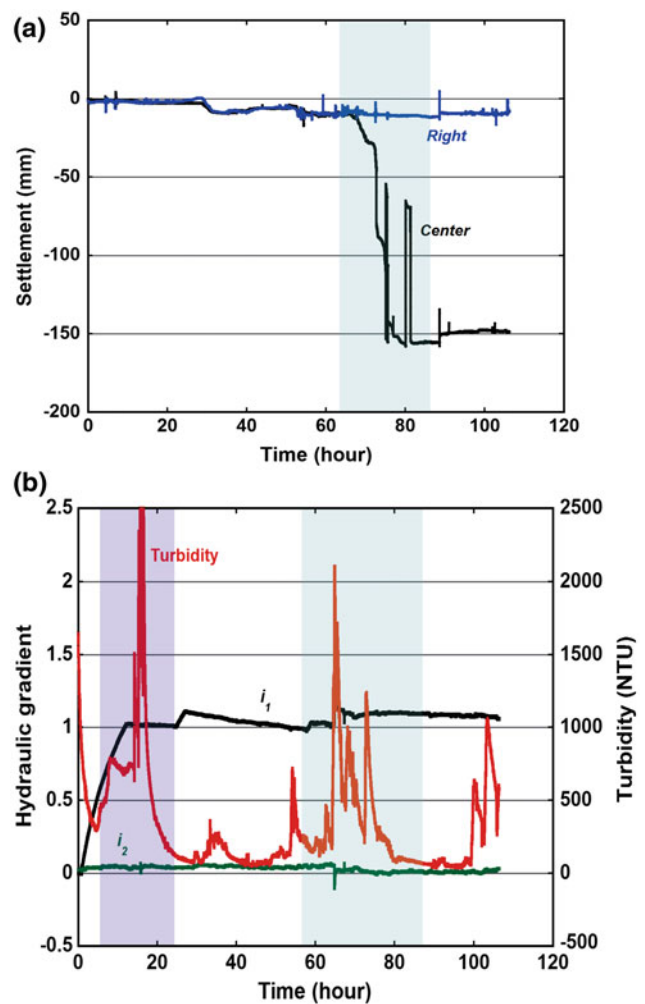

Fig. 10 Stage hydrograph and deformation mechanism of the dam model (*Experiment 3*) under steady-state flow conditions

Conclusions

A series of large-scale (outdoor) experiments were conducted with the sole purpose of investigating the premonitory factors for internal erosion and piping failure of landslide dams. The experimental scheme and the results obtained provided significant insights into the critical
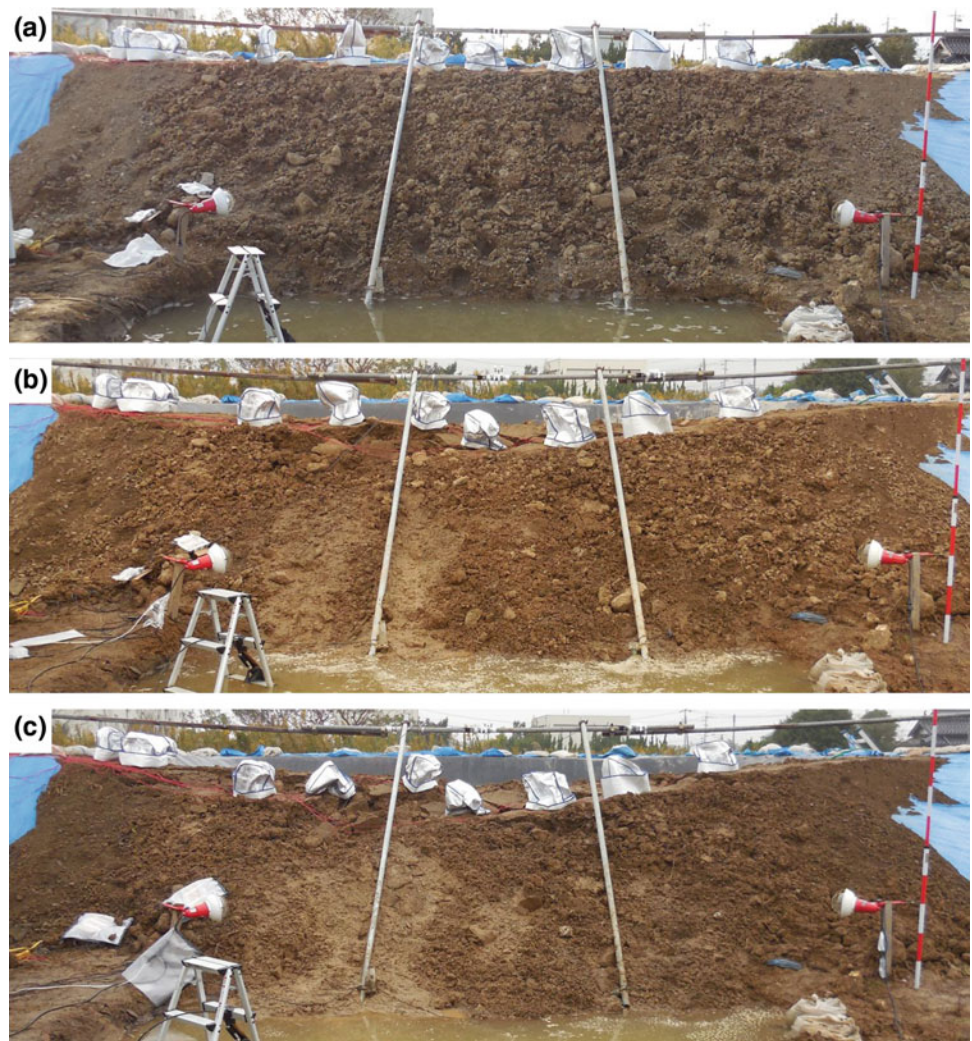
conditions for internal erosion development in landslide dams. The information obtained could aid in the development of failure time prediction models and outbreak flood hydrographs and can be employed in the study of complex sediment transport processes and other subsurface erosion processes in materials of varying physical properties.

The onset of internal erosion under steady-state seepage conditions was found to correlate with the initial internal deformations recorded by the strain gauges. A relationship was found between the rate of erosion of the dam material and the formation of concave upward depressions on the dam crests. The relative difference in the hydraulic beha-

viour and evolutionary trend of the dam models highlighted the differences in plasticity index, erodibility and other physical properties of the materials composing the dams.

This study showed that the turbidity of the seepage water can be effectively used in the prediction of the rate of internal erosion and the breaching time of landslide dams. Reasonable agreement between the negative self-potential anomalies which ranged from −18 to −20 mV (Fig. 12) and the emergence of very turbid hyperconcentrated flows from the downstream face, gives credence to the notion that turbidity can be used as an important parameter for monitoring the performance of landslide dams, and for failure time prediction.
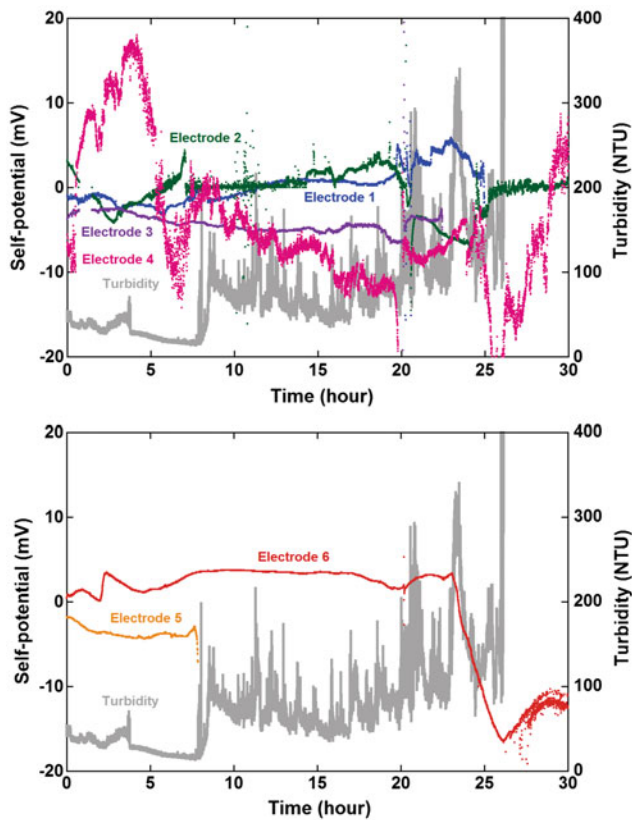
Fig. 12 Variations in turbidity and self-potential during internal erosion and piping in *Experiment 1*

References

Amaya PJ, Massey-Norton JT, Stark TD (2009) Evaluation of seepage from an embankment dam retaining fly ash. J Perform Constructed Facil 23(6):406–414

Costa JE, Schuster RL (1988) The formation and failure of natural dams. Geol Soc Am Bull 100:1054–1068

Evans SG (1986) Landslide damming in the Cordillera of western Canada. In: Landslide dams@ sProcesses, risk, and mitigation, ASCE, pp 111–130

Hermanns RL, Niedermann S, Gonzalez Diaz FE, Fauque L, Folguera A, Ivy-Ochs S, Kubik P (2004) Landslide dams in the Argentine Andes. In: NATO advanced research workshop security of natural and artificial rockslide dams, pp 79–85

Hewitt K (1982) Natural dams and outburst floods of the Karakoram Himalaya. IAHS 138:259–269

O'Connor JIME, Beebee RA (2009) 8 Floods from natural rock-material dams. Megaflooding Earth Mars 128

Ojha CSP, Singh VP, Adrian DD (2008) Assessment of the role of slit as a safety valve in failure of levees. Int J Sedim Res 23(4):361–375

Okeke ACU, Wang F (2016a) Hydromechanical constraints on piping failure of landslide dams: an experimental investigation. Geoenvironmental Disasters 3(4):1–17

Okeke ACU, Wang F (2016b) Critical hydraulic gradients for seepage-induced failure of landslide dams. Geoenvironmental Disasters 3(9):1–22

Strom A (2006) Morphology and internal structure of rockslides and rock avalanches: grounds and constraints for their modelling. Landslides from Massive Rock Slope Failure. Springer, Netherlands, pp 305–326

Strom A (2013) Geological prerequisites for landslide dams' disaster assessment and mitigation in Central Asia. In: Wang FW, Miyajima M, Li T, Wei S, Fathani TF (eds) Progress of geo-disaster mitigation technology in Asia. Springer, Berlin Heidelberg, pp 17–53

Vorogushyn S, Merz B, Apel H (2009) Development of dike fragility curves for piping and micro-instability breach mechanisms. Nat Hazards Earth Syst Sci 9(4):1383–1401